The Astrophysical Journal, 844:10 (10pp), 2017 July 20 https://doi.org/10.3847/1538-4357/aa75c9

X-Ray Bolometric Corrections for Compton-thick Active Galactic Nuclei

M. Brightman[1], M. Baloković[1], D. R. Ballantyne[2], F. E. Bauer[3,4,5], P. Boorman[6], J. Buchner[3], W. N. Brandt[7,8,9], A. Comastri[10], A. Del Moro[11], D. Farrah[12], P. Gandhi[6], F. A. Harrison[1], M. Koss[13], L. Lanz[14], A. Masini[10,15], C. Ricci[3,16], D. Stern[17], R. Vasudevan[18], and D. J. Walton[18]

[1] Cahill Center for Astrophysics, California Institute of Technology, 1216 East California Boulevard, Pasadena, CA 91125, USA
[2] Center for Relativistic Astrophysics, School of Physics, Georgia Institute of Technology, Atlanta, GA 30332, USA
[3] Instituto de Astrofísica, Facultad de Física, Pontificia Universidad Catolica de Chile, Casilla 306, Santiago 22, Chile
[4] Millennium Institute of Astrophysics (MAS), Nuncio Monseñor Sótero Sanz 100, Providencia, Santiago, Chile
[5] Space Science Institute, 4750 Walnut Street, Suite 205, Boulder, CO 80301, USA
[6] School of Physics & Astronomy, University of Southampton, Highfield, Southampton SO17 1BJ, UK
[7] Department of Astronomy and Astrophysics, 525 Davey Lab, The Pennsylvania State University, University Park, PA 16802, USA
[8] Institute for Gravitation and the Cosmos, The Pennsylvania State University, University Park, PA 16802, USA
[9] Department of Physics, 104 Davey Laboratory, The Pennsylvania State University, University Park, PA 16802, USA
[10] INAF Osservatorio Astronomico di Bologna, via Gobetti 93/3, I-40129 Bologna, Italy
[11] Max-Planck-Institut für extraterrestrische Physik, Giessenbachstrasse 1, D-85748, Garching bei München, Germany
[12] Department of Physics, Virginia Tech, Blacksburg, VA 24061, USA
[13] SNSF Ambizione Fellow, Institute for Astronomy, Department of Physics, ETH Zurich, Wolfgang-Pauli-Strasse 27, CH-8093 Zurich, Switzerland
[14] Department of Physics and Astronomy, Dartmouth College, 6127 Wilder Laboratory, Hanover, NH 03755, USA
[15] Dipartimento di Fisica e Astronomia (DIFA), Universitá di Bologna, viale Berti Pichat 6/2, I-40127 Bologna, Italy
[16] Kavli Institute for Astronomy and Astrophysics, Peking University, Beijing 100871, China
[17] Jet Propulsion Laboratory, California Institute of Technology, Pasadena, CA 91109, USA
[18] Institute of Astronomy, Madingley Road, Cambridge CB3 0HA, UK
Received 2017 March 3; revised 2017 May 17; accepted 2017 May 19; published 2017 July 17

Abstract

We present X-ray bolometric correction factors, $\kappa_{\rm Bol}$ ($\equiv L_{\rm Bol}/L_{\rm X}$), for Compton-thick (CT) active galactic nuclei (AGNs) with the aim of testing AGN torus models, probing orientation effects, and estimating the bolometric output of the most obscured AGNs. We adopt bolometric luminosities, $L_{\rm Bol}$, from literature infrared (IR) torus modeling and compile published intrinsic 2–10 keV X-ray luminosities, $L_{\rm X}$, from X-ray torus modeling of *NuSTAR* data. Our sample consists of 10 local CT AGNs, where both of these estimates are available. We test for systematic differences in $\kappa_{\rm Bol}$ values produced when using two widely used IR torus models and two widely used X-ray torus models, finding consistency within the uncertainties. We find that the mean $\kappa_{\rm Bol}$ of our sample in the range of $L_{\rm Bol} \approx 10^{42}$–$10^{45}$ erg s^{-1} is $\log_{10}\kappa_{\rm Bol} = 1.44 \pm 0.12$ with an intrinsic scatter of $\sim$0.2 dex, and that our derived $\kappa_{\rm Bol}$ values are consistent with previously established relationships between $\kappa_{\rm Bol}$ and $L_{\rm Bol}$ and $\kappa_{\rm Bol}$ and Eddington ratio ($\lambda_{\rm Edd}$). We investigate if $\kappa_{\rm Bol}$ is dependent on $N_{\rm H}$ by comparing our results on CT AGNs to published results on less-obscured AGNs, finding no significant dependence. Since many of our sample are megamaser AGNs, known to be viewed edge-on, and furthermore under the assumptions of AGN unification whereby unobscured AGNs are viewed face-on, our result implies that the X-ray emitting corona is not strongly anisotropic. Finally, we present $\kappa_{\rm Bol}$ values for CT AGNs identified in X-ray surveys as a function of their observed $L_{\rm X}$, where an estimate of their intrinsic $L_{\rm X}$ is not available, and redshift, useful for estimating the bolometric output of the most obscured AGNs across cosmic time.

Key words: galaxies: active – galaxies: nuclei – galaxies: Seyfert

1. Introduction

The bolometric luminosity, $L_{\rm Bol}$, of an accreting supermassive black hole (SMBH), otherwise known as an active galactic nucleus (AGN), describes the integrated emission from the accretion process, which traces the mass accretion rate onto the SMBH ($L_{\rm Bol} = \eta \dot{m} c^2$, where $\dot{m}$ is the mass accretion rate and η is the accretion efficiency). Thus $L_{\rm Bol}$ is an important parameter for understanding the growth of SMBHs. The emission from the accretion disk, which is the primary power generation mechanism, is reprocessed by a number of components in the vicinity of the disk, one of which is a hot corona of electrons that Compton scatters the optical and UV disk emission into the X-ray regime (e.g., Haardt & Maraschi 1991, 1993).

The fraction of the disk emission that is up-scattered into the X-ray regime is parameterized by the X-ray bolometric correction factor (from here on $\kappa_{\rm Bol}$), which is defined as $L_{\rm Bol}/L_{\rm X}$, where $L_{\rm X}$ is the X-ray luminosity in the 2–10 keV band. Many works have investigated $\kappa_{\rm Bol}$, finding that it is dependent on $L_{\rm Bol}$ (e.g., Marconi et al. 2004; Steffen et al. 2006; Hopkins et al. 2007; Lusso et al. 2012; Liu et al. 2016) and Eddington ratio ($\lambda_{\rm Edd} \equiv L_{\rm Bol}/L_{\rm Edd}$, where $L_{\rm Edd} = 4\pi\, {\rm G}\, M_{\rm BH}\, m_{\rm p} c/\sigma_{\rm T} \simeq 1.26 \times 10^{38}\, (M_{\rm BH}/M_{\odot})$ erg s^{-1} and $M_{\rm BH}$ is the mass of the black hole, e.g., Wang et al. 2004; Vasudevan & Fabian 2007, 2009; Lusso et al. 2010, 2012; Jin et al. 2012; Fanali et al. 2013; Liu et al. 2016).

Characterizing $\kappa_{\rm Bol}$ and its dependencies is important for understanding accretion physics and for estimating $L_{\rm Bol}$ when it is not possible to observe the intrinsic disk emission, but where $L_{\rm X}$ is known. This can be the case for obscured AGNs, where gas and dust in the line of sight extinguishes the optical and UV emission from the accretion disk but X-rays from the corona penetrate through (for all but the most extreme absorbing columns $N_{\rm H} < 10^{24}$ cm^{-2}). While the dependencies of $\kappa_{\rm Bol}$ have been well established for unobscured, type 1 AGNs, only

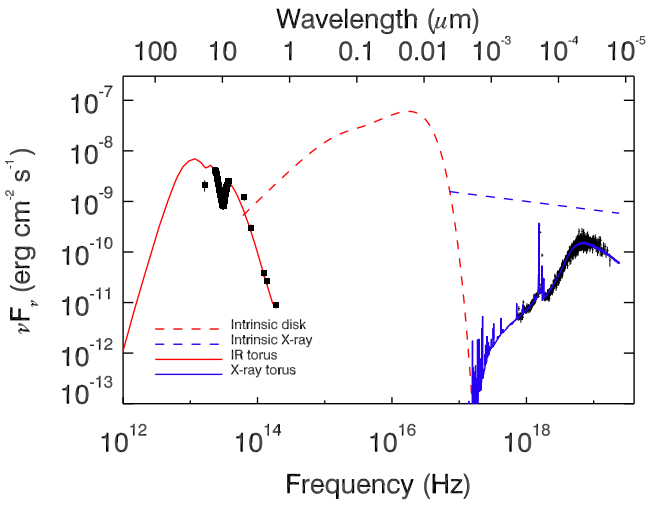

Figure 1. IR to X-ray SED of the CT AGN in the Circinus galaxy. The IR data points consist of high spatial resolution 8–13 μm spectra from the Thermal-Region Camera Spectrograph (TReCS) on Gemini-South, described in Roche et al. (2006), and high spatial resolution NIR and MIR photometry from ground-based observations and *Hubble Space Telescope*/NICMOS observations described in Alonso-Herrero et al. (2011). The solid red line is a fit to these data with the CLUMPY IR torus model of Nenkova et al. (2008) by Ichikawa et al. (2015), which yielded the $L_{\rm Bol}$ estimate. The dashed red line represents the inferred intrinsic accretion disk emission, given the known black hole mass and the inferred $L_{\rm Bol}$ from the `optxagn` model (Done et al. 2012). The X-ray data are from *NuSTAR*, described in Arévalo et al. (2014), fitted with the X-ray `torus` model by Brightman et al. (2015), plotted as a solid blue line. The intrinsic X-ray spectrum inferred from this model is plotted as a dashed blue line, from which we obtain our intrinsic $L_{\rm X}$ estimate. The gap between the dashed and solid blue lines is due to absorption.

a few studies have focussed on obscured, type 2 AGNs (e.g., Pozzi et al. 2007; Vasudevan et al. 2010; Lusso et al. 2011, 2012).

Investigating $\kappa_{\rm Bol}$ for obscured AGNs is important since the majority of AGNs in the universe are obscured (e.g., Martínez-Sansigre et al. 2005; Ueda et al. 2014; Aird et al. 2015; Buchner et al. 2015). It also has potential for testing the AGN unification scheme (e.g., Antonucci 1993; Urry & Padovani 1995), the simplest form of which describes the differences between type 1 and type 2 AGNs as solely due to orientation, where type 2 AGNs are more inclined systems and our view of the central engine is through a toroidal structure of gas and dust. The most extremely obscured sources, so-called Compton-thick (CT) AGNs ($N_{\rm H} > 1.5 \times 10^{24}\,{\rm cm}^{-2}$) constitute some ∼20%–40% of the AGN population (e.g., Brightman & Nandra 2011; Burlon et al. 2011; Brightman & Ueda 2012; Buchner et al. 2015) and host some of the most highly inclined systems, revealed through the detection of disk megamasers (Zhang et al. 2006; Masini et al. 2016). However, for CT AGNs, flux suppression is high even in the X-ray band and the effect of Compton scattering on the X-ray spectrum is dependent on the geometry of the obscuring material (e.g., Brightman et al. 2015) making the intrinsic $L_{\rm X}$ difficult to estimate. For this reason, $\kappa_{\rm Bol}$ has not previously been investigated for CT AGNs.

At energies >10 keV, while the effect of Compton scattering remains, the flux suppression is lower due to the declining photoelectric absorption cross-section with increasing energy. Therefore, *NuSTAR* (Harrison et al. 2013), with its sensitivity at these energies, is ideal for estimating the intrinsic $L_{\rm X}$ for CT AGNs. For this, X-ray spectral models that take into account the absorption and Compton scattering are needed (e.g., Ikeda et al. 2009; Murphy & Yaqoob 2009; Brightman & Nandra 2011; Liu & Li 2014). Figure 1 illustrates this point, showing the *NuSTAR* data of the well-known CT AGN in the Circinus galaxy (Arévalo et al. 2014), fitted with the Brightman & Nandra (2011) `torus` model, also showing the intrinsic X-ray spectrum inferred using the model parameters. The figure shows that a greater fraction of X-ray flux emerges above 10 keV in the source, than below 10 keV. Since its launch in 2012, *NuSTAR* has observed a large number of CT AGNs, with $L_{\rm X}$ estimated from both the `mytorus` model of Murphy & Yaqoob (2009) and the `torus` model of Brightman & Nandra (2011) by various authors (e.g., Arévalo et al. 2014; Baloković et al. 2014; Gandhi et al. 2014; Puccetti et al. 2014; Annuar et al. 2015; Bauer et al. 2015; Brightman et al. 2015; Koss et al. 2015; Rivers et al. 2015; Boorman et al. 2016; Farrah et al. 2016; Marinucci et al. 2016; Masini et al. 2016; Ricci et al. 2016).

As well as being reprocessed by the hot corona into the X-rays, the AGN disk emission is also reprocessed by the dust in the torus into the infrared (e.g., Pier & Krolik 1992). The structure of the dust torus does not necessarily have the same geometry as the X-ray absorbing material, which is gas that can exist within the dust sublimation radius. As in the X-ray band, torus models have been calculated to model the infrared emission (e.g., Nenkova et al. 2008; Hönig & Kishimoto 2010; Stalevski et al. 2012; Efstathiou et al. 2013). A natural parameter derived from these models is $L_{\rm Bol}$. Since significant infrared emission is also emitted by dusty star formation in the host galaxy, high spatial resolution IR data or broadband spectral energy distribution (SED) modeling are required to isolate the AGN and model the torus emission (e.g., Farrah et al. 2003; Stierwalt et al. 2014). Alonso-Herrero et al. (2011) presented the results from fitting of Nenkova et al. (2008) CLUMPY torus model to high spatial resolution IR spectroscopy and photometry of 13 nearby Seyfert galaxies, finding that their $L_{\rm Bol}$ estimates agreed well with other estimates from the literature. A further expanded study in the IR was conducted by Ichikawa et al. (2015), which presented an analysis of 21 nearby AGNs, with significant overlap with the sample of AGNs with X-ray torus modeling.

One such source in common is the CT AGN in the Circinus galaxy. Along with the *NuSTAR* data in Figure 1, we plot the high spatial resolution IR data along with the fit using the IR torus model. The inferred accretion disk spectrum is also shown.

The aim of this paper is to take advantage of the recent advances in both IR and X-ray torus modeling that produce estimates of $L_{\rm Bol}$ and intrinsic $L_{\rm X}$, respectively, and derive $\kappa_{\rm Bol}$ values for CT AGNs. We start in Section 2, where we describe our sample selection. In Section 3, we collect and compare results from the literature on the two widely used X-ray torus models, `mytorus` (Murphy & Yaqoob 2009) and `torus` (Brightman & Nandra 2011) and two widely used IR torus models from Fritz et al. (2006) and Nenkova et al. (2008). We assess the systematic differences, if any. Following this, we test if the $\kappa_{\rm Bol}$ values we estimate for CT AGNs are consistent with established relationships between $\kappa_{\rm Bol}$ and $L_{\rm Bol}$ and $\kappa_{\rm Bol}$ and $\lambda_{\rm Edd}$ as determined from unobscured AGNs. Next, we compare our new $\kappa_{\rm Bol}$ results for CT AGNs to results from previous studies for less obscured systems in order to explore any dependence of $\kappa_{\rm Bol}$ on $N_{\rm H}$ and probe orientation effects. We then present $\kappa_{\rm Bol}$ for CT AGNs as a function of observed $L_{\rm X}$

Table 1
Basic Properties of the Galaxies in Our Sample

Name (1)	Mag (2)	Morphology (3)	Distance (4)	M_{BH} (5)	References (6)
Circinus	10.0 (*I*)	SA(s)b?	4.2	1.7 ± 0.3	a
NGC 424	12.8 (*I*)	(R)SB0/a?(r)	50.6	...	...
NGC 1068	9.9 (*I*)	(R)SA(rs)b	14.4	8.0 ± 0.3	b
NGC 1194	12.5 (*i*)	SA$\hat{0}$ +?	58.9	65.0 ± 3.0	c
NGC 1320	12.5 (*V*)	Sa? edge-on	39.1	...	...
NGC 1386	10.76 (*R*)	SB$\hat{0}$ +(s)	15.9	1.2 ± 1.1	d
NGC 2273	10.15 (*I*)	SB(r)a?	28.9	7.5 ± 0.4	c
NGC 3079	9.5 (*I*)	SB(s)c edge-on	19.2	$2.4^{+2.4}_{-1.2}$	e
NGC 5643	10.6 (*I*)	SAB(rs)c	13.9	...	...
NGC 7582	9.2 (*I*)	(R′)SB(s)ab	22	...	...

Note. Column (1) lists the galaxy name, Column (2) gives the visual magnitude with the band in parentheses (Cousins *I*-band where available), Column (3) shows the galaxy morphology classification from NED, Coulmn (4) gives the assumed distance to the source in Mpc, and Column (5) presents M_{BH} in units of $10^6\,M_{\odot}$, where this has been estimated from the megamaser emission with the reference for this given in Column (6).
References: (a) Greenhill et al. (2003), (b) Lodato & Bertin (2003), (c) Kuo et al. (2011), (d) McConnell & Ma (2013), and (e) Kondratko et al. (2005).

and redshift, useful for studies of CT AGNs in surveys where there is not a good estimate of the intrinsic L_X. We discuss our results in Section 4 and present our conclusions in Section 5. We define L_{Bol} as the total of the inferred disk emission (from IR torus modeling) together with the intrinsic L_X (from X-ray torus modeling) in order to be consistent with previous works (e.g., Marconi et al. 2004; Vasudevan et al. 2010). We assume a flat cosmological model with $H_0 = 70\,\mathrm{km\,s^{-1}\,Mpc^{-1}}$ and $\Omega_\Lambda = 0.73$.

2. Sample Selection and Luminosity Estimates

We compile L_X measurements from X-ray torus modeling of *NuSTAR* data and L_{Bol} results from IR spectral/SED modeling from the literature, finding 10 local CT AGNs where both of these exist. We find five sources from the sample of Ichikawa et al. (2015), who used the CLUMPY torus models of Nenkova et al. (2008) to calculate L_{Bol}, fitting over the range of 1.25–30 μm. We find a further four sources from the sample of Gruppioni et al. (2016), who, rather than using high spatial resolution IR data to isolate the AGN emission, carry out SED decomposition to isolate the AGN emission from the host galaxy, using the approach described by Berta et al. (2013). They use the torus model of Fritz et al. (2006), which models a smooth distribution of dust and calculate L_{Bol} over the 1–1000 μm range. Finally, Woo & Urry (2002) calculated L_{Bol} for a large number of AGNs by simply integrating over the observed multiwavelength SED. This was a far less sophisticated approach to L_{Bol} estimation than IR torus modeling since it presumably does not account for host-galaxy emission. We compare these L_{Bol} estimates for four sources, where overlap with the IR torus modeling exists. We find one CT AGN where X-ray torus modeling has been conducted and an L_{Bol} estimate exists from Woo & Urry (2002), NGC 2273, which we include in our sample.

We list some basic observational properties of our sample in Table 1. Due to the detailed torus modeling involved, these sources are necessarily nearby ($D < 60$ Mpc). Our sample also contains six megamaser AGNs indicating that they have high inclinations, since these are required to produce this emission. Furthermore, the Keplerian motion of the masing material provides an accurate measurement of M_{BH} (e.g., Kuo et al. 2011) and allows us to test the relationship between κ_{Bol} and λ_{Edd}. We also list the M_{BH} estimates in Table 1.

The different torus models used to calculate L_X and L_{Bol} have properties that are inherent to each, which we describe here. The Nenkova et al. (2008) models assume a dust torus consisting of clouds that are distributed with axial symmetry and whose number per unit length depends on the distance from the illuminating source and the angle from the equatorial plane. This torus is illuminated by an intrinsic disk spectrum, which takes the form of a piecewise power-law distribution described in Rowan-Robinson (1995), where $\lambda F_\lambda = \lambda^{1.2}$ for $\lambda \leqslant 0.01\,\mu$m, $\lambda F_\lambda =$ constant for $0.01 \leqslant \lambda < 0.1\,\mu$m, $\lambda F_\lambda = \lambda^{-0.5}$ for $0.1 \leqslant \lambda < 1\,\mu$m, and $\lambda F_\lambda = \lambda^{-3}$ for $1\,\mu\mathrm{m} \leqslant \lambda$. Integrating over this assumed disk spectrum yields L_{Bol}. The anisotropy of this clumpy torus is discussed at length in Nenkova et al. (2008) and depends on the various parameters of the torus. For example, the torus becomes less anisotropic when the power-law index of the radial distribution of clouds increases, i.e., steeper. This is a free parameter in the model and hence fitted for in SED modeling. The anisotropy is also strongly wavelength dependent, with the torus being particularly isotropic at 12 μm.

While the Nenkova et al. (2008) model assumes a clumpy distribution of dust, the Fritz et al. (2006) model assumes smooth distribution, but that also depends on the radial distance from the source and the equatorial angle. An intrinsic disk spectrum that illuminates the torus isotropically in the form of a piecewise power-law distribution that is similar but not identical to that assumed by the Nenkova et al. (2008) models. Here $\lambda F_\lambda \propto \lambda^{1.2}$ for $0.001 \leqslant \lambda \leqslant 0.03\,\mu$m, $\lambda F_\lambda \propto$ constant for $0.03 \leqslant \lambda < 0.125\,\mu$m and $\lambda F_\lambda \propto \lambda^{-0.5}$ for $0.125 \leqslant \lambda < 20\ \mu$m. The degree of anisotropy from this torus is rather higher than for the clumpy torus, and depends on the viewing angle and the equatorial optical depth. Again these are free parameters of the model and are fitted for in SED modeling. L_{Bol} is calculated from a bolometric correction factor given the best-fit template (Gruppioni et al. 2016).

The X-ray torus models of Murphy & Yaqoob (2009) and Brightman & Nandra (2011) both model smooth distributions of gas. `mytorus` assumes a "doughnut"-like geometry with a circular cross-section, whereas the `torus` model assumes a "spherical" torus with a biconical cut out. Both models assume an intrinsic source spectrum that takes a power-law form with

Table 2
X-Ray and Bolometric Luminosities of the Sample

Name	L_X (torus)	References	L_X (mytorus)	References	L_{Bol} (IR torus)	References	L_{Bol} (SED integration)	References	κ_{Bol} (torus)	κ_{Bol} (mytorus)
(1)	(2)	(3)	(4)	(5)	(6)	(7)	(8)	(9)	(10)	(11)
Circinus	$42.51^{+0.07}_{-0.09}$	a	42.58	e	43.5 ± 0.6	i	43.60	j	1.39 ± 0.61	1.01 ± 0.67
NGC 424	$43.96^{+0.21}_{-0.16}$	a	43.50	f	44.77 ± 0.01	h	⋯		0.88 ± 0.19	1.30 ± 0.30
NGC 1068	$42.87^{+0.04}_{-0.06}$	a	43.34	g	44.4 ± 0.5	i	44.98	k	1.61 ± 0.50	1.06 ± 0.58
NGC 1194	42.56	b	42.75	b	44.74 ± 0.04	h	⋯	⋯	2.19 ± 0.30	1.98 ± 0.30
NGC 1320	$42.79^{+0.12}_{-0.09}$	a	42.85	f	44.16 ± 0.06	h	44.02	k	1.40 ± 0.12	1.36 ± 0.31
NGC 1386	$41.84^{+0.26}_{-0.05}$	a	41.30	b	42.5 ± 0.5	i	43.38	k	0.83 ± 0.52	1.33 ± 0.58
NGC 2273	$43.11^{+0.19}_{-0.34}$	b	42.60	b	⋯	⋯	44.05	k	1.04 ± 0.40	1.52 ± 0.42
NGC 3079	$41.53^{+0.45}_{-0.43}$	a	42.15	b	43.61 ± 0.25	h	⋯	⋯	2.09 ± 0.51	1.49 ± 0.39
NGC 5643	41.90	c	41.95	c	43.00 ± 0.5	i	⋯	⋯	1.02 ± 0.58	0.98 ± 0.58
NGC 7582	41.70	d	41.54	d	43.50 ± 0.5	i	⋯	⋯	1.85 ± 0.58	2.00 ± 0.58

Note. Column (1) lists the AGN name, Column (2) presents the logarithm of the intrinsic 2–10 keV luminosity in erg s^{-1} estimated from the `torus` model of Brightman & Nandra (2011), with references listed in Column (3). Column (4) presents the logarithm of the intrinsic 2–10 keV luminosity in erg s^{-1} estimated from the `mytorus` model of Murphy & Yaqoob (2009), with references listed in Column (5). Column (6) lists the logarithm of the bolometric luminosity in erg s^{-1} estimated from IR torus modeling, with references in Column (7). Column (8) list the logarithm of the bolometric luminosity in erg s^{-1} estimated from SED integration with references in Column (9). Column (10) lists the logarithm of κ_{Bol} when using the L_X measurement from the `torus` model and L_{Bol} from the IR torus modeling, corrected for distance discrepancies between the two, and Column (11) lists the logarithm of κ_{Bol} when using the L_X measurement from the `mytorus` model, also using L_{Bol} from the IR torus modeling, corrected for distance discrepancies.
References: (a) Brightman et al. (2015), (b) Masini et al. (2016)/private communication, (c) Annuar et al. (2015), (d) Rivers et al. (2015), (e) Arévalo et al. (2014), (f) Baloković et al. (2014), (g) Bauer et al. (2015), (h) Gruppioni et al. (2016), (i) Ichikawa et al. (2015), (j) Moorwood et al. (1996), (k) Woo & Urry (2002).

$F_\gamma \propto E^{-\Gamma}$ ($\lambda F_\lambda = E^{-\Gamma+2}$). For sight lines through the torus, the anisotropy in the *NuSTAR* band is negligible.

The luminosities that we have compiled here are a collection of literature values that also depend on the distance assumed by each author, which can often have large discrepancies due to the nearby nature of these galaxies. For example, Brightman et al. (2015) assume a distance of 6.2 Mpc to the Circinus galaxy based on the Hubble flow distance for the intrinsic L_X estimate from the `torus` model, whereas Arévalo et al. (2014) assume a distance of 4.2 Mpc based on the Tully estimate for the intrinsic L_X estimate from the `mytorus` model. Furthermore, Ichikawa et al. (2015) assume a distance of 4 Mpc for the L_{Bol} estimate. Since luminosity scales with distance squared, this difference leads to a factor of ∼2 discrepancy, which we must account for when calculating and comparing κ_{Bol} values. We do this by taking the luminosity and the distance assumed by each author and correcting the luminosity assuming the distance that we list in Table 1.

We list the intrinsic L_X and L_{Bol} estimates in Table 2 along with the corresponding κ_{Bol} values, which have been corrected for distance. Our sample spans a range of $L_X \approx 10^{41.5}$–10^{44} erg s^{-1}, $L_{Bol} \approx 10^{42}$–10^{45} erg s^{-1}, $M_{BH} \approx 10^6 - 7 \times 10^7\ M_\odot$, and $\lambda_{Edd} \approx$ 0.01–0.3. All our sources are Compton thick by selection with $N_H = 10^{24}$–10^{25} cm^{-2}, with the exception of NGC 1320, which has $N_H > 10^{25}$ cm^{-2} (Brightman et al. 2015).

3. X-Ray Bolometric Corrections for CT AGNs

With L_X and L_{Bol} estimates from different methods for the 10 CT AGNs, our first step is to investigate the κ_{Bol} values derived using each of these. Figure 2 shows the individual κ_{Bol} values for each CT AGN and for each combination of L_X and L_{Bol}. The uncertainties shown correspond to the uncertainties in L_X and L_{Bol} combined in quadrature. Where no uncertainty is available, we assume a value of 0.3 dex, which is typical of our sample. We also show the mean of each combination,

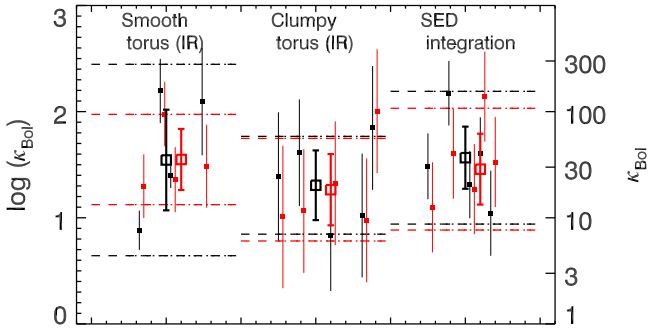

Figure 2. Individual κ_{Bol} values (small squares ordered from left to right as they are ordered top to bottom in Table 1) calculated from the `torus` (black) and `mytorus` (red) models, given L_{Bol} estimated from the smooth IR torus model (left), the clumpy IR torus model (middle) and from simple SED integration (right). The large empty squares show the mean of these values when taking into account intrinsic scatter, where the error bars represent the 1σ uncertainty in the mean. The dotted lines show the estimated standard deviation of the intrinsic scatter.

calculated assuming that there is an intrinsic underlying Gaussian scatter in κ_{Bol}. The error bars represent the uncertainty in the mean. We also plot our estimate of the intrinsic scatter (1σ) in Figure 2, which we find to be $\log\kappa_{Bol} \sim 0.5$ (with large uncertainties).

For the X-ray torus modeling, there is no evidence for a systematic difference in the mean κ_{Bol} values estimated from each model. This is true whether using the estimates of L_{Bol} from Ichikawa et al. (2015), Gruppioni et al. (2016), or Woo & Urry (2002). Furthermore, when considering source by source estimates, all κ_{Bol} estimates agree within the uncertainties when comparing the results from the X-ray torus models. We also find no evidence for a systematic difference in κ_{Bol} values between the different L_{Bol} estimates. We find that all the κ_{Bol} values, regardless of which X-ray or IR torus modeling is used,

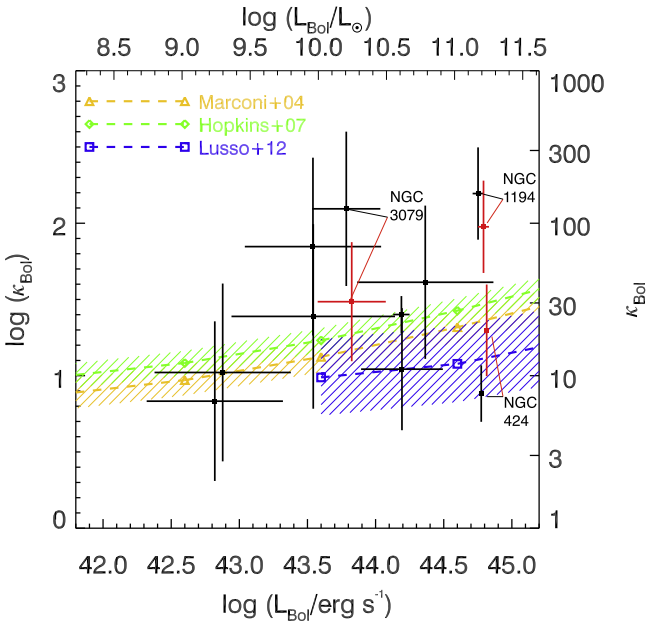

Figure 3. X-ray bolometric corrections for the CT AGN vs. $L_{\rm Bol}$, where $L_{\rm X}$ has been estimated from the `torus` model (black points). We show our results with respect to the published relationships from Marconi et al. (2004), Hopkins et al. (2007), and Lusso et al. (2012). Dashed regions show their 1σ intrinsic dispersions. For most sources, the measurements agree with the relationships. However, for NGC 424 and NGC 3079, $\kappa_{\rm Bol}$ given the $L_{\rm X}$ estimate from the `mytorus` model provides a better agreement, which we plot in red, shifted to slightly higher $L_{\rm Bol}$ values for clarity. For NGC 1194, both estimates lie significantly away from the relationships.

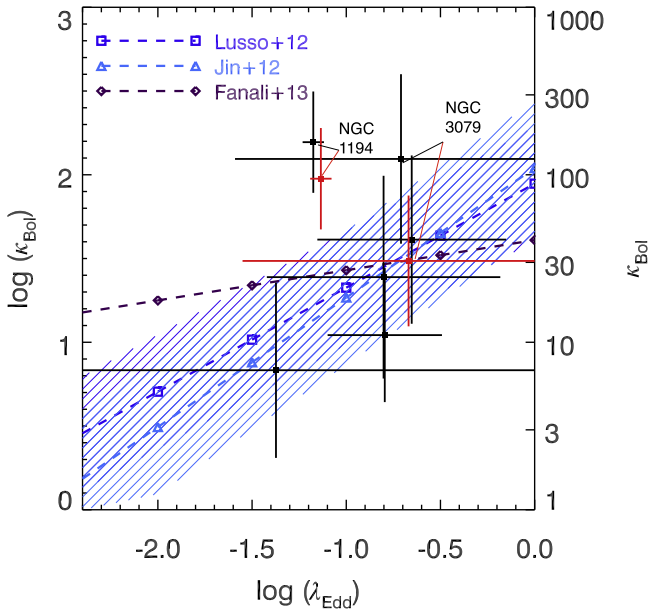

Figure 4. X-ray bolometric corrections for the CT AGN vs. $\lambda_{\rm Edd}$, where $L_{\rm X}$ has been estimated from the `torus` model (black data points). We also plot the relationships from Lusso et al. (2012), Jin et al. (2012), and Fanali et al. (2013). Dashed regions show their 1σ intrinsic dispersions (no measure of the dispersion is presented by Fanali et al. 2013). Similarly, for our comparison with relationships for $L_{\rm Bol}$, we find that most of our measurements agree for both X-ray models and that NGC 1194 lies significantly above the relationships.

even simple SED integration, are statistically consistent with each other.

Since there are well established relationships between $\kappa_{\rm Bol}$ and $L_{\rm Bol}$ and $\kappa_{\rm Bol}$ and $\lambda_{\rm Edd}$, we proceed to test our derived $\kappa_{\rm Bol}$ values by comparing to these relationships. For this, we investigate estimates of $\kappa_{\rm Bol}$ when using either $L_{\rm X}$ from the `torus` model and $L_{\rm X}$ from the `mytorus` model. We plot our $\kappa_{\rm Bol}$ values against $L_{\rm Bol}$ in Figure 3 along with the relationships presented in Marconi et al. (2004), Hopkins et al. (2007) and Lusso et al. (2012) and their intrinsic dispersions. With regards to the dependence of $\kappa_{\rm Bol}$ on $\lambda_{\rm Edd}$, we plot our results with the previously reported relationships between these quantities from Lusso et al. (2012), Jin et al. (2012) and Fanali et al. (2013) in Figure 4.

For most sources, the measurements agree with the relationships for both $L_{\rm X}$ measurements. However, for NGC 424 and NGC 3079, the $\kappa_{\rm Bol}$ values given the $L_{\rm X}$ estimate from the `mytorus` model provide better agreement. For NGC 1194, both estimates lie significantly away from the relationships, $\sim 2\sigma$ for the `torus` model and $\sim 1.5\sigma$ for the `mytorus` model. For our analysis of $\kappa_{\rm Bol}$, henceforth, we use the $L_{\rm X}$ estimate from the `torus` model with the exception of NGC 424 and NGC 3079, where we use the $L_{\rm X}$ estimate from the `mytorus` model. For NGC 1194, the fact that neither $L_{\rm X}$ estimates are in agreement with the relationships may imply that the intrinsic $L_{\rm X}$ has been underestimated by ~ 0.5 dex. Alternatively, $L_{\rm Bol}$ may have been overestimated by the same amount. We discuss and investigate the inclusion of NGC 1194 in our sample in later analyses.

While many previous works have calculated $\kappa_{\rm Bol}$ for unobscured AGNs and obscured but Compton-thin AGNs, this is the first time systematic calculations of $\kappa_{\rm Bol}$ for CT AGNs have been carried out. By combining our results with those for unobscured AGNs and Compton-thin AGNs, this allows us to investigate if $\kappa_{\rm Bol}$ is dependent on $N_{\rm H}$, and over a wider range than was previously possible. In the context of the standard AGN unification model, whereby higher obscurations correspond to larger viewing angles through the torus, probing the dependence of $\kappa_{\rm Bol}$ on $N_{\rm H}$ will allow us to test orientation effects. Specifically, we will explore if the fraction of the accretion disk emission reprocessed by the corona into the X-rays is orientation dependent.

For unobscured AGNs and Compton-thin obscured AGNs, we again use the large sample of $L_{\rm Bol}$ estimates from IR torus SED fitting presented in Gruppioni et al. (2016), the parent sample of which was the extended 12 micron galaxy sample by Rush et al. (1993). Absorption column measurements, $N_{\rm H}$ and intrinsic $L_{\rm X}$ values for a large subset of this sample was presented in Brightman & Nandra (2011) from an X-ray spectral analysis of *XMM-Newton* data. In order to do a comparison that is as direct as possible, we restrict our comparison to sources that have the same range in $L_{\rm Bol}$ as our sources, i.e., $L_{\rm Bol} \approx 10^{42}$–$10^{45}$ erg s^{-1}, a total of 21 sources.

We plot $\kappa_{\rm Bol}$ against $N_{\rm H}$ combining our results on CT AGNs with the results from unobscured and Compton-thin AGNs in Figure 5. In order to investigate the dependence of $\kappa_{\rm Bol}$ on $N_{\rm H}$, we calculate mean $\kappa_{\rm Bol}$ values for three bins in $N_{\rm H}$, $\log(N_{\rm H}/{\rm cm}^{-2}) = 20$–$22$, 22–24, and 24–26, and estimate the intrinsic scatter assuming it to be a Gaussian centered on the mean, finding that $\log_{10}\kappa_{\rm Bol} = 1.36 \pm 0.44$, $\log_{10}\kappa_{\rm Bol} = 1.54 \pm 0.20$, and $\log_{10}\kappa_{\rm Bol} = 1.44 \pm 0.12$, respectively, with an intrinsic scatter of $\sim$0.2–1 dex. The mean $\kappa_{\rm Bol}$ values are all within 1–2σ of each other implying that there is no strong dependence of $\kappa_{\rm Bol}$ on $N_{\rm H}$.

Among the unobscured AGNs, NGC 6810 appears to be an extreme outlier with $\kappa_{\rm Bol} > 3000$. Here it is possible that $L_{\rm Bol}$

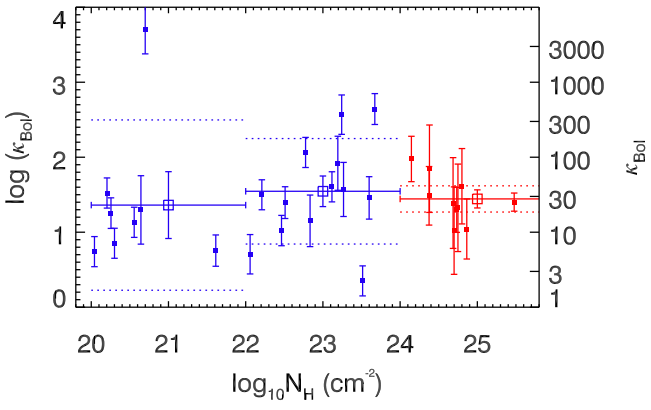

Figure 5. Individual κ_{Bol} values as a function of N_H for our CT AGN sample (small filled red squares) combined with data from unobscured and Compton-thin AGNs from Gruppioni et al. (2016) and Brightman & Nandra (2011; small filled blue squares) selected to have the same range of L_{Bol} as our sample. The large empty squares represent the means of these data points for three bins in N_H, and the dotted lines mark the estimated σ of the intrinsic scatter. The extreme outlier is NGC 6810, where it is likely that L_{Bol} from SED fitting has been severely overestimated.

estimated through SED fitting in Gruppioni et al. (2016) has been overestimated since these authors find that the L_{Bol} estimate from the [Ne V] and [O IV] lines are more than a magnitude less than that from SED fitting. We therefore consider the effect of excluding this source from further analysis.

For us to put an estimate on the anisotropy of the corona, we assume that our CT AGNs are viewed edge-on and that sources with $\log(N_H/\mathrm{cm}^{-2}) = 20$–22 are viewed face-on. Since many of our CT AGNs are megamaser sources, which are required to be viewed at high inclination, our first assumption is well motivated. To assume that unobscured AGNs are viewed face-on, we must invoke the unification scheme. We then define anisotropy as the fraction of L_X emitted by unobscured AGNs to that emitted by CT AGNs given the same L_{Bol}. This simply equates to

$$\text{anisotropy} \equiv \frac{\kappa_{Bol}(\log_{10}(N_H/\mathrm{cm}^{-2}) = 24 - 26)}{\kappa_{Bol}(\log_{10}(N_H/\mathrm{cm}^{-2}) = 20 - 22)}. \quad (1)$$

Given our data, we find this to be 1.2 (1σ confidence range = 0.4–3.5), suggesting that the corona emits ~1.2 times more in polar directions with respect to equatorial directions with a 1σ upper limit of 3.5 times. If we were to exclude the outliers NGC 1194 and NGC 6810 from our analysis of the anisotropy, we would find that the anisotropy is 2.1 (1.4–3.2). Our results imply that the X-ray corona is not strongly anisotropic.

3.1. κ_{Bol} as a Function of Observed L_X and Redshift

The κ_{Bol} values that we have derived here for CT AGNs can be used to estimate bolometric luminosities; however, this is only the case when a good estimate of the intrinsic L_X is available. This requires relatively good, high-energy X-ray data, for example, from *NuSTAR*, in order to conduct X-ray torus modeling to account for the reprocessing effects of the Compton-thick obscuring medium. Such data will be available for a large number of local Seyfert 2s from modeling by M. Baloković et al. (2017, in preparation).

The all-sky *Swift*/BAT survey has become a popular resource for detecting and identifying CT AGNs in the local universe. For example, Ricci et al. (2015) and Akylas et al. (2016) identify ~50 CT AGNs in the 70-month *Swift*/BAT catalog (Baumgartner et al. 2013), also presenting intrinsic L_X values from torus modeling. For the seven sources in our sample that have been detected by *Swift*/BAT, we determine that the mean κ_{Bol} given the intrinsic 14–195 keV L_X estimates from Ricci et al. (2015) is 1.12 ± 0.17 with an intrinsic scatter estimated to be 0.30 ± 0.25.

In addition, Koss et al. (2016) presented a method for identifying local CT AGNs in low-quality *Swift*/BAT spectra. Since it is difficult to estimate intrinsic L_X for these sources, we explore κ_{Bol} for the observed 14–195 keV luminosity. We compile observed L_X(14–195 keV) values for the seven CT AGNs in our sample that were detected by *Swift*/BAT. We then calculate the bolometric correction factors for these observed luminosities using the L_{Bol} values presented in Table 2, which we find to be 1.70 ± 0.19 with an intrinsic scatter estimated to be 0.36 ± 0.21.

While *Swift*/BAT has detected and identified numerous CT AGNs in the local universe, the high spatial resolution and sensitivity of *Chandra*, *XMM-Newton*, and *NuSTAR* are better suited for detecting these sources at higher redshift. For example, Brightman & Ueda (2012) and Brightman et al. (2014) have identified ~100 CT AGNs candidates up to $z \sim 4$ in the deep *Chandra* observations of the CDFS, AEGIS-XD, and C-COSMOS fields. However, due to the low-count nature of these sources, spectral parameters are difficult to constrain well, not least the intrinsic L_X. Intrinsic L_X estimates are usually obtained by fixing one or more spectral parameters, such as Γ and the opening angle of the torus, θ_{tor}, to canonical values (e.g., 1.9 for Γ and 60° for θ_{tor}) . However, spectral analysis of CT AGNs with *NuSTAR* have revealed a wide variety of spectral shapes and complexity that is neglected when assuming a simple spectral model as described above.

We therefore use the best-fit models of our 10 sources, which includes the range of spectral parameters observed and all spectral complexity such as a scattered power-law component, to calculate the observed *Chandra* luminosity that would be seen were they observed at higher redshifts. Our broadband *NuSTAR* spectra are essential for this since they tell us what *Chandra* is observing at these epochs. For example, at $z = 2$, the observed 0.5–8 keV *Chandra* bandpass corresponds to restframe 1.5–24 keV, the expected flux in which is straightforward to calculate from our *NuSTAR* spectra.

We then define a bolometric correction to this observed luminosity,

$$\kappa'_{Bol} \equiv \frac{L_{Bol}}{L(0.5 - 8\ \mathrm{keV}, \text{observed})} \quad (2)$$

and calculate this for each source from its X-ray spectrum and known L_{Bol} for a range of redshifts. We include in the L_{Bol} value the intrinsic L_X, despite the fact that the bolometric correction is to the observed L_X. We then calculate the mean of this κ'_{Bol} from all 10 sources at each redshift. Figure 6 shows this mean κ'_{Bol} and its corresponding 1σ spread for redshifts up to $z = 6$. Table 3 gives these numbers for ease of interpretation.

A small number of CT AGNs have also been identified in the *NuSTAR* surveys of the same fields above (e.g., Civano et al. 2015; A. Del Moro et al. 2017, in preparation; L. Zapacosta et al. 2017, in preparation), and as such, we also carry out the same

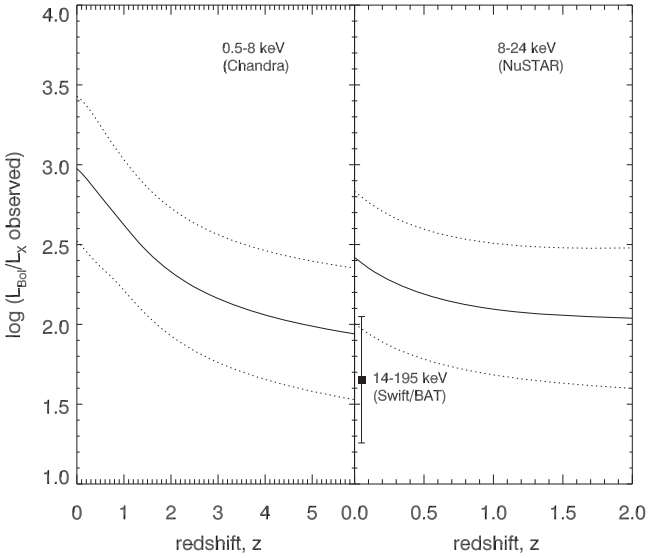

Figure 6. Mean bolometric corrections (solid lines) with 1σ spread (dotted lines) for the CT AGNs in our sample given the observed *Chandra* 0.5–8 keV (left) and *NuSTAR* 8–24 keV (right) luminosities as a function of redshift. We also show the *Swift*/BAT $\kappa_{\rm Bol}$ value for our sample at low redshift.

calculations as above, but for the observed 8–24 keV $L_{\rm X}$, and also present these values in Figure 6. Since the restframe 8–24 keV band can only be observed with *NuSTAR* up to $z = 2$ (restframe 24 keV corresponds to observed 72 keV, which is at the end of the *NuSTAR* bandpass), we only show up to this redshift.

The main caveat involved with this method is that our sample contains relatively low luminosity AGNs. Since the typical luminosities of CT AGNs detected and identified at high-redshift are ≈1–2 orders of magnitude more luminous than ours, luminosity effects must be taken into account. First, the distribution of spectral parameters are expected to be different at higher luminosities, for example, $\theta_{\rm tor}$ is expected to be larger (Brightman et al. 2015). This is a relatively small effect, however, and not larger than the 1σ range of values presented in Figure 6. Second, the known relationship between $\kappa_{\rm Bol}$ and $L_{\rm Bol}$ (Figure 3) means that $\kappa_{\rm Bol}$ is systematically higher for these more luminous AGNs. The median $L_{\rm Bol}$ of our sample is $\sim 10^{44}$ erg s^{-1} ($\sim 10^{10.5}\,L_{\odot}$). For the most luminous AGNs (e.g., $L_{\rm Bol} \gtrsim 10^{46}$ erg s^{-1}) $\kappa_{\rm Bol}$ is a factor of ≈6 greater than at the luminosities of our sample, which should be taken into account. Since the dependence of $\kappa_{\rm Bol}$ on $L_{\rm Bol}$ is well known, it can be used to correct the estimated $L_{\rm Bol}$.

For example, if we were to consider a source at $z = 2$ with an observed 0.5–8 keV luminosity of 10^{44} erg s^{-1}, from Figure 6, we would estimate its $L_{\rm Bol}$ as 2.5×10^{46} erg s^{-1} (i.e., log $(\kappa'_{\rm Bol}) \approx 2.4$). For this $L_{\rm Bol}$ value, the relationship presented by Marconi et al. (2004) would predict $\kappa_{\rm Bol} \approx 60$. Since the mean $\kappa_{\rm Bol}$ of our lower luminosity sample is ≈25, the original $L_{\rm Bol}$ estimate of 2.5×10^{46} erg s^{-1} should be corrected upward by a factor of $\frac{60}{25} = 2.4$, making $L_{\rm Bol} \sim 6 \times 10^{46}$ erg s^{-1}.

4. Discussion

In our calculation of $\kappa_{\rm Bol}$ for CT AGNs, we have investigated different methods for estimating both $L_{\rm X}$ and $L_{\rm Bol}$ for these heavily obscured sources, finding that the results

Table 3
Mean Bolometric Corrections as a Function of Redshift

Redshift	$\log_{10}L_{\rm Bol}/L$(0.5–8 keV)	$\log_{10}L_{\rm Bol}/L$(8–24 keV)
0.0	2.976 ± 0.454	2.418 ± 0.415
0.1	2.948 ± 0.457	2.353 ± 0.412
0.2	2.914 ± 0.457	2.299 ± 0.409
0.3	2.878 ± 0.455	2.254 ± 0.408
0.4	2.841 ± 0.450	2.219 ± 0.407
0.5	2.804 ± 0.442	2.189 ± 0.407
0.6	2.766 ± 0.432	2.163 ± 0.407
0.7	2.731 ± 0.424	2.143 ± 0.408
0.8	2.695 ± 0.417	2.124 ± 0.409
0.9	2.660 ± 0.413	2.109 ± 0.411
1.0	2.622 ± 0.409	2.095 ± 0.412
1.1	2.587 ± 0.407	2.085 ± 0.414
1.2	2.551 ± 0.405	2.075 ± 0.416
1.3	2.518 ± 0.404	2.068 ± 0.419
1.4	2.486 ± 0.402	2.061 ± 0.421
1.5	2.456 ± 0.402	2.056 ± 0.424
1.6	2.427 ± 0.401	2.051 ± 0.427
1.7	2.401 ± 0.401	2.047 ± 0.430
1.8	2.375 ± 0.400	2.044 ± 0.433
1.9	2.351 ± 0.400	2.042 ± 0.437
2.0	2.329 ± 0.400	2.039 ± 0.440
2.1	2.307 ± 0.400	2.038 ± 0.444
2.2	2.287 ± 0.400	2.037 ± 0.448
2.3	2.269 ± 0.400	2.035 ± 0.451
2.4	2.251 ± 0.400	2.034 ± 0.455
2.5	2.233 ± 0.400	2.034 ± 0.459
2.6	2.218 ± 0.400	2.033 ± 0.463
2.7	2.203 ± 0.400	2.033 ± 0.467
2.8	2.189 ± 0.400	2.033 ± 0.471
2.9	2.174 ± 0.400	2.034 ± 0.475
3.0	2.162 ± 0.400	2.034 ± 0.479
3.1	2.150 ± 0.401	2.033 ± 0.483
3.2	2.138 ± 0.401	2.036 ± 0.486
3.3	2.126 ± 0.401	2.047 ± 0.488
3.4	2.115 ± 0.401	2.056 ± 0.490
3.5	2.105 ± 0.402	2.065 ± 0.492
3.6	2.095 ± 0.402	2.075 ± 0.494
3.7	2.086 ± 0.402	2.085 ± 0.496
3.8	2.076 ± 0.403	2.096 ± 0.498
3.9	2.067 ± 0.403	2.105 ± 0.499
4.0	2.059 ± 0.403	2.115 ± 0.501
4.1	2.051 ± 0.404	2.125 ± 0.503
4.2	2.043 ± 0.404	2.135 ± 0.505
4.3	2.035 ± 0.405	2.145 ± 0.507
4.4	2.027 ± 0.405	2.156 ± 0.508
4.5	2.021 ± 0.405	2.165 ± 0.510
4.6	2.014 ± 0.406	2.175 ± 0.511
4.7	2.007 ± 0.406	2.185 ± 0.513
4.8	2.001 ± 0.407	2.195 ± 0.515
4.9	1.994 ± 0.407	2.206 ± 0.517
5.0	1.988 ± 0.408	2.217 ± 0.519
5.1	1.983 ± 0.408	2.226 ± 0.520
5.2	1.977 ± 0.409	2.236 ± 0.522
5.3	1.971 ± 0.409	2.246 ± 0.523
5.4	1.966 ± 0.410	2.257 ± 0.525
5.5	1.960 ± 0.410	2.268 ± 0.527
5.6	1.955 ± 0.411	2.280 ± 0.529
5.7	1.950 ± 0.411	2.290 ± 0.530
5.8	1.945 ± 0.412	2.300 ± 0.531
5.9	1.941 ± 0.412	2.311 ± 0.533

Note. A tabulated version of Figure 6 for easier interpretation.

are generally insensitive to the toroidal geometry assumed for the obscurer in both the infrared and X-rays. We also used established relationships between $\kappa_{\rm Bol}$ and $L_{\rm Bol}$ and $\kappa_{\rm Bol}$ and $\lambda_{\rm Edd}$ to test our derived $\kappa_{\rm Bol}$ values finding that they agreed well, implying that the torus modeling recovers these intrinsic parameters well. This is significant considering that the geometries assumed by the models differ, which is especially the case between the X-ray and IR models. Regarding a comparison of the torus models in the infrared, Feltre et al. (2012) conducted a comparison of the Fritz et al. (2006) and Nenkova et al. (2008) IR torus models, which were used to obtain our $L_{\rm Bol}$ estimates. These two models assume different dust distributions, smooth and clumpy respectively. Feltre et al. (2012) found that while the two models can produce similarly shaped SEDs, the underlying parameters derived, such as the covering factor, are different. However, in terms of the $L_{\rm Bol}$ values derived from these models, we do not find a statistically significant difference between the models.

Nevertheless, a few exceptions to this were found. We found that for NGC 424 and NGC 3079, the $L_{\rm X}$ estimate from the `mytorus` model gave a $\kappa_{\rm Bol}$ value that is in better agreement with the relationships. For NGC 1194, our $\kappa_{\rm Bol}$ estimates lie significantly above the relationships by $\sim$0.5 dex. This could be due to a systematic underestimation of the intrinsic $L_{\rm X}$, possibly caused by the underestimation of $N_{\rm H}$. Alternatively, this could have been caused by an overestimation of $L_{\rm Bol}$ in the SED fitting by Gruppioni et al. (2016), perhaps due to contamination by star formation in the host galaxy. Finally, it is possible that the $\kappa_{\rm Bol}$ value for NGC 1194 lies at the extreme of the intrinsic ditribution of $\kappa_{\rm Bol}$ for its luminosity. Figure 5 shows that similarly high $\kappa_{\rm Bol}$ values are found for the less obscured sources too.

We note that there are differences in the relationships between $\kappa_{\rm Bol}$ and $L_{\rm Bol}$ presented by Marconi et al. (2004), Hopkins et al. (2007), and Lusso et al. (2012), some of which are to do with the definition of $L_{\rm Bol}$. Marconi et al. (2004) define their intrinsic bolometric luminosities as the sum of the optical and UV emission from the accretion disk and X-ray emission from the corona. Hopkins et al. (2007) follow a similar approach to Marconi et al. (2004); however, they count the IR emission that is reprocessed disk emission. For this reason, the Hopkins et al. (2007) relation is systematically higher than the Marconi et al. (2004) one. Lusso et al. (2012) use the sum of the AGN IR (1–1000 μm) and X-ray (0.5–100 keV) luminosities as a proxy for the intrinsic nuclear luminosity. Since they only count the reprocessed emission, their $\kappa_{\rm Bol}$ estimates should be comparable to Marconi et al. (2004). However, it is lower. Lusso et al. (2012) discuss this finding, suggesting that since their sample is X-ray selected, it is biased toward X-ray bright sources that have lower $\kappa_{\rm Bol}$ values. We note that the differences in the established relationships are smaller than our uncertainties, so we cannot say which relationships our data agree with better. Regarding our methods for the CT AGNs and their less obscured counterparts, we follow the same approach as Marconi et al. (2004) in that we take $L_{\rm Bol}$ to be the sum of the inferred optical and UV emission (from IR torus modeling) and X-ray emission.

We have also found that the intrinsic $\kappa_{\rm Bol}$ values for CT AGNs is statistically consistent with $\kappa_{\rm Bol}$ for less obscured AGNs indicating that there is little dependence of $\kappa_{\rm Bol}$ on $N_{\rm H}$. Under the assumption of the standard AGN unification model, whereby for unobscured sources the central engine is viewed face-on and for heavily obscured sources it is viewed edge-on, this then implies that the fraction of X-rays emitted with respect to the optical/UV emission from the disk does not have a strong dependence on the orientation of the X-ray emitting corona. Since our sample contains many megamasers, which are known to be viewed edge-on, this supports our assumption based on unification. The lack of a strong dependence on orientation is important for understanding the physics of the disk-corona system, since it implies the corona emits almost isotropically, while the disk is known to emit anisotropically (Netzer 1987). The models of You et al. (2012) and Xu (2015) predict a weak dependence of the optical to X-ray slope, $\alpha_{\rm OX}$ (which is strongly correlated with $\kappa_{\rm Bol}$) on orientation. Since the predicted difference appears to be $<$0.1 dex in $\kappa_{\rm Bol}$, and we place a 1σ upper limit of 3.5 on this difference, the predictions of the models are not possible to detect with our current data.

Anisotropic X-ray emission would have possible implications for the AGN obscured fraction. Sazonov et al. (2015) proposed that collimation of X-rays in the polar direction (i.e., that observed in unobscured type 1 AGNs) could lead to the observed dependence of the obscured fraction on $L_{\rm X}$, and that potentially the intrinsic obscured fraction has no luminosity dependence as observed. This, however, would require a strong dependence of $L_{\rm X}$ on viewing angle, α, following the cosine law, i.e., $dL/d\Omega \propto \cos\alpha$, such that $L_{\rm X}$ drops to zero for edge-on viewing angles. While our results allow for a factor of 3.5 drop from face-on to edge-on, they are inconsistent with the cosine law, albeit with a small sample. Similarly, Brightman et al. (2016) found that megamaser CT AGNs show the same relationship between the X-ray spectral index, Γ, and $\lambda_{\rm Edd}$ as do unobscured AGNs, further arguing against anisotropic X-ray emission.

Isotropic X-ray radiation, on the other hand, is also supported by the observed tight correlation between the X-ray and infrared luminosities that is statistically the same for both type 1 and type 2 AGNs (e.g., Gandhi et al. 2009; Asmus et al. 2015), unless both the IR and X-rays emit anisotropically in the same direction (Yang et al. 2015).

While we have found that the $\kappa_{\rm Bol}$ values for our sample of relatively low luminosity CT AGNs are consistent with the relationship found for unobscured AGNs in the same luminosity range, our sample lacks the high luminosity sources required to confirm if the increasing trend of $\kappa_{\rm Bol}$ with $L_{\rm Bol}$ holds for CT AGNs. One such highly luminous ($L_{\rm Bol} \sim 10^{47}$ erg s^{-1}) close to Compton thick ($N_{\rm H} \sim 5 \times 10^{23}$ cm^{-2}) source, IRAS 09104+4109, where similar X-ray and IR torus modeling has been carried out, exists (Farrah et al. 2016). These authors estimate $L_{\rm X}$ to be 1–2 $\times$ 10^{45} erg s^{-1} and $L_{\rm Bol}$ to be $\sim$1.8 $\times$ 10^{47} erg s^{-1} implying that $\kappa_{\rm Bol} \sim 100$. This value agrees very well with the relationship found for unobscured AGNs suggesting that there is agreement between heavily obscured AGNs and unobscured AGNs across a wide range in luminosities.

5. Summary and Conclusions

We have compiled intrinsic $L_{\rm X}$ and $L_{\rm Bol}$ values for a sample of 10 local CT AGNs from IR and X-ray torus modeling and have investigated $\kappa_{\rm Bol}$ for these heavily obscured sources for the first time. We find the following.

1. There are no statistically significant differences in $\kappa_{\rm Bol}$ values when using the X-ray torus models of Murphy & Yaqoob (2009) or Brightman & Nandra (2011) to calculate $L_{\rm X}$ or the infrared torus models of Fritz et al. (2006) or Nenkova et al. (2008) to calculate $L_{\rm Bol}$.
2. Our $\kappa_{\rm Bol}$ estimates for CT AGNs are consistent with the established relationships between $\kappa_{\rm Bol}$ and $L_{\rm Bol}$ in the range of $L_{\rm Bol} \approx 10^{42}$–$10^{45}$ erg s^{-1} and $\kappa_{\rm Bol}$ and $\lambda_{\rm Edd}$ in the range of $\lambda_{\rm Edd} \approx 0.01$–$0.3$. However, we find that for NGC 424 and NGC 3079 the $L_{\rm X}$ estimates from the `mytorus` model provide better agreement. For NGC 1194, our $\kappa_{\rm Bol}$ estimate is too high considering both the $L_{\rm Bol}$ or $\lambda_{\rm Edd}$ relationships. This may imply that the intrinsic $L_{\rm X}$ has been underestimated by $\sim$0.5 dex or that $L_{\rm Bol}$ has been overestimated by the same amount.
3. There is no evidence that $\kappa_{\rm Bol}$ depends on $N_{\rm H}$. Under the assumptions of AGN unification, whereby the most obscured AGNs are viewed edge-on and unobscured AGNs are viewed face-on, this implies that the X-ray emission from the corona does not depend strongly on viewing angle. We estimate an upper limit on the anisotropy of the corona, finding that it emits no more than 3.5 times (1σ confidence level) in polar directions than in equatorial directions, albeit based on a small sample.
4. We have presented $\kappa_{\rm Bol}$ for CT AGNs as a function of the observed $L_{\rm X}$ and redshift, useful for estimating $L_{\rm Bol}$ of CT AGNs identified in X-ray surveys where a good measurement of the intrinsic $L_{\rm X}$ is not available.

We thank the referee for providing a constructive review of our manuscript, which improved its quality. We also thank Kohei Ichikawa for insights into IR torus modeling and Almudena Alonso-Herrero and Pat Roche for providing the IR data for Figure 1. M. Baloković acknowledges support from NASA Headquarters under the NASA Earth and Space Science Fellowship Program, grant NNX14AQ07H. We acknowledge financial support from the ASI/INAF grant I/037/12/0–011/13 (A.C., A.M.) and the Caltech Kingsley visitor program (A.C.). This work was supported under NASA Contract No. NNG08FD60C and made use of data from the *NuSTAR* mission, a project led by the California Institute of Technology, managed by the Jet Propulsion Laboratory, and funded by the National Aeronautics and Space Administration. We thank the *NuSTAR* Operations, Software, and Calibration teams for support with the execution and analysis of these observations. Furthermore, this research has made use of the NASA/IPAC Extragalactic Database (NED), which is operated by the Jet Propulsion Laboratory, California Institute of Technology, under contract with the National Aeronautics and Space Administration.

Facility: NuSTAR.

References

Aird, J., Coil, A. L., Georgakakis, A., et al. 2015, MNRAS, 451, 1892
Akylas, A., Georgantopoulos, I., Ranalli, P., et al. 2016, A&A, 594, A73
Alonso-Herrero, A., Ramos Almeida, C., Mason, R., et al. 2011, ApJ, 736, 82
Annuar, A., Gandhi, P., Alexander, D. M., et al. 2015, ApJ, 815, 36
Antonucci, R. 1993, ARA&A, 31, 473
Arévalo, P., Bauer, F. E., Puccetti, S., et al. 2014, ApJ, 791, 81
Asmus, D., Gandhi, P., Hönig, S. F., Smette, A., & Duschl, W. J. 2015, MNRAS, 454, 766
Baloković, M., Comastri, A., Harrison, F. A., et al. 2014, ApJ, 794, 111
Bauer, F. E., Arévalo, P., Walton, D. J., et al. 2015, ApJ, 812, 116
Baumgartner, W. H., Tueller, J., Markwardt, C. B., et al. 2013, ApJS, 207, 19
Berta, S., Lutz, D., Santini, P., et al. 2013, A&A, 551, A100
Boorman, P. G., Gandhi, P., Alexander, D. M., et al. 2016, ApJ, 833, 245
Brightman, M., Baloković, M., Stern, D., et al. 2015, ApJ, 805, 41
Brightman, M., Masini, A., Ballantyne, D. R., et al. 2016, ApJ, 826, 93
Brightman, M., & Nandra, K. 2011, MNRAS, 413, 1206
Brightman, M., Nandra, K., Salvato, M., et al. 2014, MNRAS, 443, 1999
Brightman, M., & Ueda, Y. 2012, MNRAS, 423, 702
Buchner, J., Georgakakis, A., Nandra, K., et al. 2015, ApJ, 802, 89
Burlon, D., Ajello, M., Greiner, J., et al. 2011, ApJ, 728, 58
Civano, F., Hickox, R. C., Puccetti, S., et al. 2015, ApJ, 808, 185
Done, C., Davis, S. W., Jin, C., Blaes, O., & Ward, M. 2012, MNRAS, 420, 1848
Efstathiou, A., Christopher, N., Verma, A., & Siebenmorgen, R. 2013, MNRAS, 436, 1873
Fanali, R., Caccianiga, A., Severgnini, P., et al. 2013, MNRAS, 433, 648
Farrah, D., Afonso, J., Efstathiou, A., et al. 2003, MNRAS, 343, 585
Farrah, D., Baloković, M., Stern, D., et al. 2016, ApJ, 831, 76
Feltre, A., Hatziminaoglou, E., Fritz, J., & Franceschini, A. 2012, MNRAS, 426, 120
Fritz, J., Franceschini, A., & Hatziminaoglou, E. 2006, MNRAS, 366, 767
Gandhi, P., Horst, H., Smette, A., et al. 2009, A&A, 502, 457
Gandhi, P., Lansbury, G. B., Alexander, D. M., et al. 2014, ApJ, 792, 117
Greenhill, L. J., Kondratko, P. T., Lovell, J. E. J., et al. 2003, ApJL, 582, L11
Gruppioni, C., Berta, S., Spinoglio, L., et al. 2016, MNRAS, 458, 4297
Haardt, F., & Maraschi, L. 1991, ApJL, 380, L51
Haardt, F., & Maraschi, L. 1993, ApJ, 413, 507
Harrison, F. A., Craig, W. W., Christensen, F. E., Hailey, C. J., & Zhang, W. W. 2013, ApJ, 770, 103
Hönig, S. F., & Kishimoto, M. 2010, A&A, 523, A27
Hopkins, P. F., Richards, G. T., & Hernquist, L. 2007, ApJ, 654, 731
Ichikawa, K., Packham, C., Ramos Almeida, C., et al. 2015, ApJ, 803, 57
Ikeda, S., Awaki, H., & Terashima, Y. 2009, ApJ, 692, 608
Jin, C., Ward, M., & Done, C. 2012, MNRAS, 425, 907
Kondratko, P. T., Greenhill, L. J., & Moran, J. M. 2005, ApJ, 618, 618
Koss, M. J., Assef, R., Baloković, M., et al. 2016, ApJ, 825, 85
Koss, M. J., Romero-Cañizales, C., Baronchelli, L., et al. 2015, ApJ, 807, 149
Kuo, C. Y., Braatz, J. A., Condon, J. J., et al. 2011, ApJ, 727, 20
Liu, Y., & Li, X. 2014, ApJ, 787, 52
Liu, Z., Merloni, A., Georgakakis, A., et al. 2016, MNRAS, 459, 1602
Lodato, G., & Bertin, G. 2003, A&A, 398, 517
Lusso, E., Comastri, A., Simmons, B. D., et al. 2012, MNRAS, 425, 623
Lusso, E., Comastri, A., Vignali, C., et al. 2010, A&A, 512, A34
Lusso, E., Comastri, A., Vignali, C., et al. 2011, A&A, 534, A110
Marconi, A., Risaliti, G., Gilli, R., et al. 2004, MNRAS, 351, 169
Marinucci, A., Bianchi, S., Matt, G., et al. 2016, MNRAS, 456, L94
Martínez-Sansigre, A., Rawlings, S., Lacy, M., et al. 2005, Natur, 436, 666
Masini, A., Comastri, A., Baloković, M., et al. 2016, A&A, 589, A59
McConnell, N. J., & Ma, C.-P. 2013, ApJ, 764, 184
Moorwood, A. F. M., Lutz, D., Oliva, E., et al. 1996, A&A, 315, L109
Murphy, K. D., & Yaqoob, T. 2009, MNRAS, 397, 1549
Nenkova, M., Sirocky, M. M., Nikutta, R., Ivezić, Ž, & Elitzur, M. 2008, ApJ, 685, 160
Netzer, H. 1987, MNRAS, 225, 55
Pier, E. A., & Krolik, J. H. 1992, ApJ, 401, 99
Pozzi, F., Vignali, C., Comastri, A., et al. 2007, A&A, 468, 603
Puccetti, S., Comastri, A., Fiore, F., et al. 2014, ApJ, 793, 26
Ricci, C., Bauer, F. E., Treister, E., et al. 2016, ApJ, 819, 4
Ricci, C., Ueda, Y., Koss, M. J., et al. 2015, ApJL, 815, L13
Rivers, E., Baloković, M., Arévalo, P., et al. 2015, ApJ, 815, 55
Roche, P. F., Packham, C., Telesco, C. M., et al. 2006, MNRAS, 367, 1689
Rowan-Robinson, M. 1995, MNRAS, 272, 737
Rush, B., Malkan, M. A., & Spinoglio, L. 1993, ApJS, 89, 1
Sazonov, S., Churazov, E., & Krivonos, R. 2015, MNRAS, 454, 1202
Stalevski, M., Fritz, J., Baes, M., Nakos, T., & Popović, L. C. 2012, MNRAS, 420, 2756
Steffen, A. T., Strateva, I., Brandt, W. N., et al. 2006, AJ, 131, 2826
Stierwalt, S., Armus, L., Charmandaris, V., et al. 2014, ApJ, 790, 124
Ueda, Y., Akiyama, M., Hasinger, G., Miyaji, T., & Watson, M. G. 2014, ApJ, 786, 104
Urry, C. M., & Padovani, P. 1995, PASP, 107, 803
Vasudevan, R. V., & Fabian, A. C. 2007, MNRAS, 381, 1235
Vasudevan, R. V., & Fabian, A. C. 2009, MNRAS, 392, 1124

Vasudevan, R. V., Fabian, A. C., Gandhi, P., Winter, L. M., & Mushotzky, R. F. 2010, MNRAS, 402, 1081
Wang, J.-M., Watarai, K.-Y., & Mineshige, S. 2004, ApJL, 607, L107
Woo, J.-H., & Urry, C. M. 2002, ApJ, 579, 530
Xu, Y.-D. 2015, MNRAS, 449, 191
Yang, H., Wang, J., & Liu, T. 2015, ApJ, 799, 91
You, B., Cao, X., & Yuan, Y.-F. 2012, ApJ, 761, 109
Zhang, J. S., Henkel, C., Kadler, M., et al. 2006, A&A, 450, 933